

Contents list available at CBIORE journal website

Renewable Energy Development

Journal homepage: https://ijred.cbiore.id



Research Article

Optimization of ultrasonication time on the production of ZnO-SiO₂ nanocomposite as photocatalytic material

Lailatul Qomariyah^a, Nurul Faizah^a, Achmad Dwitama Karisma^a, Sulthan Rabbani^a, Sultan Hendra Mahardi Kalloka^a, Nicky Rahmana Putra^bo,

Abstract. Nanocomposite ZnO-SiO2 is widely known for its efficacy as a semiconductor photocatalyst. Current nanocomposite production methods face challenges like particle agglomeration and inconsistent particle size control. To overcome this problem, the ultrasonication method was used to prevent agglomeration and produce composites in nanoscale, where this study synthesized ZnO-SiO2 for photocatalytic degradation of dye color. To prepare this nanocomposite, the ultrasonication time was varied from 0 to 45 minutes to understand the particle properties and the effectivity on the photocatalytic activity. Silica was prepared from water glass via sol-gel method to produce colloidal SiO2 nanoparticles and then mixed with ZnO with the ratio of 3% wt and subjected to ultrasonication method. Under various ultrasonication time, the FTIR analysis shows the Si-O peak at 895 cm⁻¹ indicates the presence of SiO₂ particles. The XRD validate the formation of ZnO-SiO₂ nanoparticles, supporting the FTIR analysis. The best nanoparticle properties were achieved with 45 minutes of ultrasonication. The SEM analysis confirms the present of SiO₂ and ZnO. From BET analysis, ZnO-SiO₂ has a high surface area (117.64 m²/g), moderate pore volume (0.46 cm³/g), and small particle pore size (11.59 nm). The photocatalytic activity of ZnO-SiO₂ nanocomposites was evaluated by the degradation of methylene blue (MB) under sunlight and the best performance reached by the nanocomposite prepared under 45 minutes ultrasonication. The results show that the ultrasonication technique efficiently reduces agglomeration, as indicated by a reduction in particle diameter from 35.04 nm (pure ZnO) to 11.59 nm (ZnO-SiO2), and significantly enhances photocatalytic activity, achieving 97% degradation of MB under sunlight after 180 minutes. The aforementioned technique demonstrates significant potential for industrial use, providing higher efficiency and expandability in manufacturing superior photocatalytic substances.

Keywords: ZnO-SiO₂; semiconductor; photocatalytic; ultrasonic; agglomeration.



@ The author(s). Published by CBIORE. This is an open access article under the CC BY-SA license (http://creativecommons.org/licenses/by-sa/4.0/). Received: 24th March 2025; Revised: 17th May 2025; Accepted: 24th June 2025; Available online: 18th July 2025

Introduction

Environmental pollution, particularly the release of harmful substances from industrial effluents, represents a serious risk to ecosystems and human well-being. Among the various pollutants, organic compounds such as dyes, pharmaceuticals, and pesticides are especially concerning due to their persistence and resistance to natural degradation processes. These pollutants are often released into water bodies from industries such as textiles, pharmaceuticals, and food processing, where conventional wastewater treatment methods may not efficiently remove them. Consequently, the search for more effective, sustainable, and environmentally friendly solutions has become a pressing global concern (El Golli et al., 2023). In this context, the adoption of non-thermal and green processing technologies has shown promise in enhancing extraction and functional performance of natural materials without compromising structural integrity (Faizah et al., 2024). Semiconductor photocatalysts have emerged as one of the most potential technologies for degrading organic pollutants. They offer the advantage of utilizing sunlight or UV light to activate the breakdown of harmful substances into less toxic or inert

byproducts (El Golli et al., 2023). Zinc oxide (ZnO) is one of the most widely studied semiconductor photocatalysts because of its excellent photocatalytic activity, strong chemical stability, and non-toxic properties, and long-term photostability (Lee & Abd Hamid, 2015). ZnO band gap was 3.37 eV and a binding energy of 60 meV, making it suitable for applications under UV light exposure. Interestingly, ZnO's oxidation properties often exceed those of TiO2 under UV light, as ZnO can absorb a broader UV spectrum (Joshaghani et al., 2017). ZnO has demonstrated significant potential for degrading various organic compounds under UV or sunlight irradiation.

Despite its promising photocatalytic performance, ZnO faces practical challenges that limit its efficiency in real-world applications. One of the main issues is particle agglomeration, where ZnO nanoparticles tend to cluster together, leading to a reduction in surface area and a loss of active sites for photocatalytic reactions. Additionally, controlling the particle size of ZnO is crucial, as nanoscale particles provide higher surface-to-volume ratios, which are essential for enhancing photocatalytic activity. Inconsistent particle size distribution can lead to uneven performance and reduced effectiveness in

^aDepartment of Industrial Chemical Engineering, Institut Teknologi Sepuluh Nopember, Surabaya, 60111, Indonesia

 $[^]b$ Faculty of Science Technology and Engineering, Higher College of Technology, Ruwais, Abu Dhabi, United Arab Emirates

Corresponding author Email: laila.qomariyah@its.ac.id (L. Qomariyah)

pollutant degradation. To further enhance the photocatalytic performance of ZnO, surface modifications such as doping with metals or non-metals, as well as forming composite materials, have been widely explored (Elbanna *et al.*, 2016). Recent developments in material design have shown that the choice of synthesis method significantly influences the structural, morphological, and surface properties of photocatalytic materials (Faizah & Qomariyah, 2024).

One particularly effective modification strategy is the incorporation of silicon dioxide (SiO2) into ZnO to form ZnO-SiO₂ nanocomposites. SiO₂ has been widely used as a doping material due to its thermal stability and ability to serve as a support for catalysts (Wang et al., 2014). In ZnO-SiO₂ composites, SiO₂ enhances the structural stability of the nanocomposite and increases its surface area, leading to improved photocatalytic performance (Stanley et al., 2019). The interaction between ZnO and SiO2 facilitates better charge separation, thereby reducing electron-hole recombination and increasing photocatalytic efficiency under UV irradiation (Winardi et al., 2020; Pratiwi et al, 2024). However, achieving uniform particle size and preventing agglomeration during the synthesis of ZnO-SiO₂ nanocomposites is challenging, as traditional methods of nanocomposite production often result in large agglomerates that negatively impact photocatalytic performance. To overcome these challenges, ultrasonication has been recognized as a potent method for enhancing the synthesis of nanocomposites, including ZnO-SiO₂ (Rohilla et al., 2021; Winardi et al., 2020).

Ultrasonication involves the application of high-frequency sound waves to a liquid medium, creating microscopic bubbles that collapse violently, generating intense localized energy (Asadi *et al.*, 2019). This process, known as cavitation, helps to break up particle agglomerates and ensures that the nanoparticles remain uniformly dispersed throughout the solution (Selvinsimpson *et al.*, 2021). Additionally, ultrasonication can assist in controlling the size and distribution of nanoparticles, producing composites with more consistent and desirable properties. The technique is relatively simple, cost-effective, and scalable, making it a valuable tool for the production of nanomaterials with enhanced properties.

The objective of this study is to determine the ideal ultrasonication duration that achieves a balance between particle size reduction, enhanced surface area, and reduced agglomeration, ultimately improving the photocatalytic efficiency of the nanocomposite for degrading organic pollutants. By optimizing ultrasonication time, this study seeks to address the challenges related to particle dispersion and agglomeration, ensuring consistent performance in photocatalytic applications.

2. Materials and Method

2.1 Materials

Zinc acetate, methanol, sodium hydroxide (NaOH), hydrochloric acid (HCl), Amberlite 120R cation exchange resin, and water glass (sodium silicate solution) were used as raw materials. All chemicals were of analytical grade and used without further purification. Distilled water was used throughout the experimental procedures.

2.2 Preparation of SiO2 and ZnO Precursors

Silica nanoparticles were prepared from water glass using the sol-gel method. The water glass solution was first diluted with distilled water, then passed through a cation exchange column packed with HCl-activated Amberlite 120R resin to remove sodium ions. The resulting solution was stirred while 0.1 M NaOH was added dropwise until the pH reached 11, resulting in a 3 wt% colloidal silica solution.

For ZnO precursor preparation, zinc acetate was dissolved in 100 mL of methanol. NaOH was added dropwise under constant stirring until pH 11 was achieved. The colloidal SiO_2 was then mixed into the ZnO precursor solution under continuous mechanical stirring.

2.3 Synthesis of ZnO-SiO₂ Nanocomposite via Ultrasonication

The combined ZnO-SiO₂ mixture was subjected to ultrasonication using a probe-type ultrasonic processor for 0, 10, 20, 30, and 45 minutes. The acoustic cavitation induced by ultrasonication improved mass transfer. reduced agglomeration, and promoted uniform distribution of ZnO over the SiO₂ matrix. 0 min means the nanocomposite was prepared under mechanical stirring. After sonication, the suspension was allowed to settle, filtered, washed with deionized water, and dried at 120 °C for 6 hours. The novelty of this study lies in the systematic investigation of the effect of varying ultrasonication time on the synthesis of ZnO-SiO₂ composite. The impact of ultrasonication time on the structural, spectral, and surface characteristic of the composite was examined, concentrating on the dispersion of ZnO onto SiO₂, the crystallite size, and the photocatalytic performance. The optimal ultrasonication duration was identified based on the highest photocatalytic degradation of MB solution.

2.4 Characterization Technique (FTIR, XRD, SEM, BET)

X-ray diffraction (XRD) was used to confirm the crystalline phases of ZnO and SiO_2 in the composite, and to evaluate the effect of sonication time on crystallinity. XRD was employed to confirm the crystal phase and estimate crystallite size of the nanocomposite. The average crystallite size (D) of $\mathrm{ZnO}\mathrm{-SiO}_2$ was calculated using the Scherrer equation (Eq 1):

$$D = \frac{k\lambda}{\beta \cos \theta} \tag{1}$$

where D is the average crystallite size (nm), k is a constant (0.94), λ represents the CuK α radiation wavelength (0.15418 nm), β denotes the Full-Width at Half-Maximum (FWHM), and θ is half the diffraction angle of the highest peak.

Fourier Transform Infrared Spectroscopy (FTIR) was employed to identify functional groups and chemical bonding within the composite. Scanning Electron Microscopy (SEM) was used to analyze the morphology and elemental composition of the composite, emphasizing the impact of ultrasonication time on particle distribution and agglomeration. Brunauer-Emmett-Teller (BET) analysis was performed to determine the surface area of the composite, assessing the effect of different sonication times on the surface properties of the photocatalyst.

2.5 Photocatalytic Activity Test

The photocatalytic activity of the $ZnO-SiO_2$ composites was evaluated by the degradation of methylene blue (MB) under visible light irradiation. The experiments were conducted by dispersing 200 mg of composite in an MB solution. At first, the mixture was put in a low-light environment for 30 minutes to examine composite's adsorption behavior. Then, followed by exposure to direct sunlight, with periodic sampling every 30 minutes to monitor the degradation rate using UV-Vis spectrophotometry. We calculated the evolution of photocatalytic degradation efficiency using equation (2):

$$\eta(\%) = \frac{c_0 - c_t}{c_0} x 100 \tag{2}$$

where η , C_0 , C_t represents the efficiency of photocatalytic as a function of time, the initial concentration of MB, and the concentration of MB at time t, respectively.

2.6 Kinetic Modelling Calculation

The pseudo-first order kinetic model was adapted to determine the kinetics of photodegradation using equation 4.

$$\ln\frac{c_t}{c_0} = -kt \tag{3}$$

where k is the rate constant. The kinetic study was performed by plotting $\ln \frac{c_t}{c_0}$ against t, in which the value of k equals to the negative gradient.

3. Result And Discussion

3.1. Molecular Structure of the Produce Nanocomposite

Figure 1 is the molecular structure of the $\rm ZnO\textsc{-}SiO_2$ nanocomposite. $\rm SiO_2$ will form a chemical bond with the surface atoms of $\rm ZnO$. This interaction can be in the form of covalent and ionic bonds. $\rm SiO_2$ can form a Si-O-Zn bond where oxygen bridges between the silicon and zinc atoms. This bridge can be formed from electron sharing (covalent) and electrostatic attraction between the Si and Zn atoms (ionic). The combination of $\rm ZnO$ and $\rm SiO_2$ in the nanocomposite can enhance the properties of both materials. $\rm SiO_2$ can stabilize the nanocomposite, thereby improving the dispersion and transmission properties of light, while $\rm ZnO$ can provide its photocatalytic activity in the nanocomposite (Kurnaz Yetim et al., 2020).

The Si–O–Zn linkage is crucial for anchoring ZnO particles onto the silica matrix, enhancing the stability and dispersion of ZnO in the composite (M. Wang et al., 2019). Additionally, SiO₂ contributes a mesoporous, high-surface-area framework that enhances light harvesting and facilitates the exposure of active photocatalytic sites (Alothman, 2012). The abundant surface hydroxyl groups (–OH) on SiO₂ further promote strong interactions with polar dye molecules such as methylene blue, thereby enhancing adsorption and subsequent degradation (Shaba et al., 2023). From an electronic standpoint, the heterojunction formed via Si–O–Zn linkages facilitate charge transfer across the interface and reduces electron–hole recombination. The presence of band offsets and localized

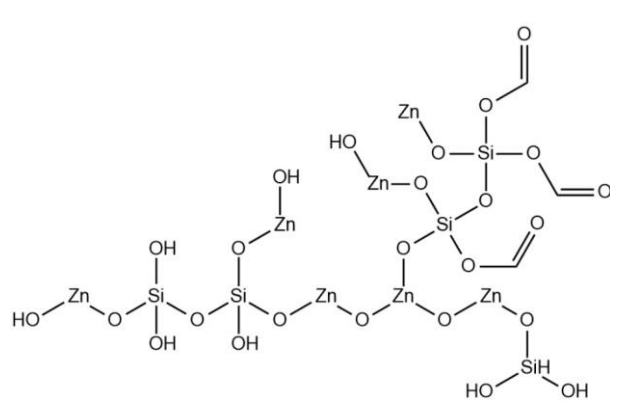


Fig 1 Molecular Structure of ZnO-SiO₂

electric fields at the ZnO–SiO₂ interface supports more efficient charge separation, which significantly enhances photocatalytic performance under solar irradiation (Ortiz-Quiñonez & Pal, 2024). Overall, such interfacial engineering strategies are recognized as key to improving the stability and activity of photocatalytic nanocomposites.

3.2. Fourier Transform Infrared (FTIR) Analysis: Functional Groups, Ultrasonication Effects, and Particle Homogeneity

Characterization of the ZnO-SiO₂ nanocomposite has been conducted using FTIR analysis, as shown in Fig. 2, which indicates that ZnO-SiO₂ particles have been successfully synthesized, evidenced by the presence of Zn-O and SiO₂ chemical bonds. The spectra confirm successful formation of the composite, indicated by the presence of both Zn-O and Si-O-Si vibrational modes. The FTIR spectra revealed a distinct peak at 895 cm⁻¹, corresponding to the asymmetric stretching vibration of Si-O-Si bonds, confirming the presence of SiO₂ nanoparticles. A prominent peak at 895 cm⁻¹ corresponds to the asymmetric stretching vibration of the Si-O-Si bond, confirming the incorporation of SiO2 into the nanocomposite matrix. The increase in O-H peak intensity with longer ultrasonication time suggests greater hydroxyl group exposure, which enhances the hydrophilicity and potential interaction sites for dye molecules (Chen et al., 2017). Notably, an increase in ultrasonication time led to a progressive sharpening of the O-H stretching band (typically observed near 3400 cm⁻¹), indicating greater exposure of hydroxyl functional groups on the surface. This suggests an increase in available active sites for dye adsorption (Kadir et al., 2023). In the variation of sonication time in Figure 2, it is noted that an increase in sonication time leads to longer exposure, the sharper the resulting O-H peak. This observation highlights the role of ultrasonication in enhancing particle dispersion and exposing new surface functionalities, indicating that the ultrasonication process plays a role in the dispersion and homogenization of particles. The cavitation effect generated by ultrasonic waves facilitates the uniform distribution of SiO₂ and prevents agglomeration, leading to improved surface uniformity and particle interaction (Asadi et al., 2019). Consequently, the O-H groups can disperse and adhere to the surface of ZnO, as evidenced by the steeper O-H peak in the FTIR graph. These hydroxyl groups enhance

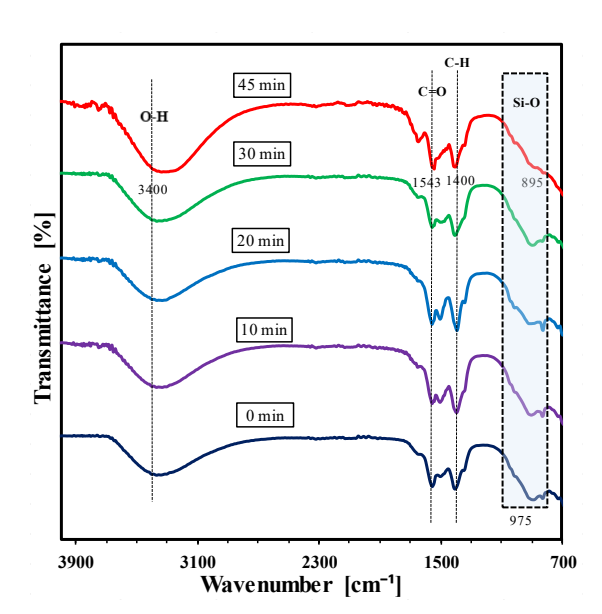


Fig 2. FTIR spectra of ZnO-SiO₂

the nanocomposite's hydrophilicity, which is critical for efficient photocatalytic degradation of polar pollutants such as methylene blue (Shaba *et al.*, 2023). This occurs due to the formation of groups of hydroxyl on the new surface, along with the increased surface area of the material (Chen *et al.*, 2017).

The influence of ultrasonication parameters on the nanocomposite structure is observable in the FTIR spectra, where shifts in peak intensities—particularly O–H and Si–O–Zn groups—can be attributed to the influence of ultrasonic energy input on the material's molecular structure. Study from (Kadir et al., 2023) found that ultrasonication at a wave amplitude of 25% still resulted in agglomerated particles, whereas wave amplitudes of 50% and 75% produced spherical particle structures that were cohesive and free from agglomeration. This outcome highlights the critical role of ultrasonic energy input in determining the structural uniformity of nanomaterials. Ultrasonication operates through the phenomenon of acoustic cavitation, wherein rapid formation and violent collapse of microscopic gas bubbles within the liquid medium generate localized hotspots characterized by transient high temperature and pressure. These extreme microenvironments not only drive physical effects such as microstreaming, shear forces, and turbulence but also induce chemical effects including free radical formation and molecular bond breakage (Wang et al., 2018; Xu et al., 2021). The input ultrasonic energy—comprising parameters such as frequency, power, and duration—critically influences these cavitation phenomena and hence the extent and nature of physical and chemical interactions occurring within the system (Qu et al., 2012). Higher ultrasonic energy enhances cavitation intensity, leading to more effective disruption and reorganization of nanomaterial structures, resulting in improved dispersion and structural uniformity. However, excessive energy might result in undesirable effects like over-fragmentation or structural degradation, highlighting the need for optimized energy input (Jin et al., 2015; Ren et al., 2014).

Furthermore, the spatial positioning of cavitation bubbles relative to solid particles also influences the morphological outcome. When cavitation occurs near the surface of solid particles, it produces asymmetric collapse patterns and intense shear forces that effectively erode and fragment particle agglomerates. In contrast, cavitation in bulk liquid generates more turbulent flow fields, contributing to the reshaping of ZnO particles into varied morphologies (Mahdavi & Ashraf Talesh, 2017) The ability to fine-tune these conditions underscores the versatility of ultrasonication in producing nanocomposites with tailored physicochemical properties. Photocatalytic activity is significantly influenced by hydroxyl ions and crystal size (Cheng et al., 2019). According to (Mourya et al., 2023), crystalline and morphology significantly affect photocatalytic efficiency by regulating properties such as surface area and charge carrier mobility, which in turn determine the photocatalytic activity of the material.

3.3. X-ray Diffraction (XRD) Analysis: Crystallinity, SiO₂-Induced Crystal Growth Suppression, and Interfacial Electron Effects

The formation of ${\rm SiO_2}$ particles also confirmed by XRD analysis, as shown in Fig. 3, where the ZnO peaks correspond to JCPDS No. 005-0664, which has a wurtzite crystal system. The diffraction peaks at $2\theta=31.7^{\circ}$, 34.4° , 36.2° , 47.5° , 56.5° , 62.8° , 66.4° , and 69.0° match well with the hexagonal wurtzite structure of ZnO (JCPDS No. 005-0664), assigned to the (100), (002), (101), (102), (110), (103), (200), (112), and (201) planes respectively. The amorphous structure of ${\rm SiO_2}$ reduces the intensity of the ZnO crystals (Ali et al., 2016). The presence of

amorphous SiO₂ results in a significant decrease in the intensity of ZnO diffraction peaks, suggesting partial shielding or dilution of crystalline domains (Holder & Schaak, 2019). The decrease in the ZnO peaks caused by the amorphous structure of SiO₂, where an increasing composition of SiO2 disrupts the crystallinity of ZnO. As the SiO₂ content increases, it interferes with the nucleation and growth of ZnO crystallites, causing peak broadening and intensity reduction, which reflects the decline in long-range crystalline order (Chen et al., 2017; Raha & Ahmaruzzaman, 2022). The ZnO peaks decrease as the concentration of SiO₂ increases, attributed to the SiO₂ structure of amorphous affecting the crystals of ZnO (Shaba et al., 2023). This effect has also been associated with the spatial separation of ZnO domains by SiO₂ layers, leading to more isolated and nanoscale ZnO regions (N. Wang et al., 2011; X. Wang et al., 2013).

Based on the XRD analysis, the crystallite size of the synthesized ZnO-SiO2 nanocomposite with 3 wt% SiO2 was calculated to be approximately 7 nm. This size is significantly smaller compared to typical pure ZnO nanoparticles, which often exhibit crystallite sizes ranging from 20 to 30 nm depending on the synthesis method (Bindu & Thomas, 2014). The incorporation of 3 wt% SiO₂ into the ZnO matrix led to a reduction in crystallite size, consistent with the suppressive effect of the amorphous silica phase on ZnO crystal growth and aggregation. This is due to the addition of SiO2 in the nanocomposite, which causes the ZnO nanoparticles to expand, thereby forming new bonds, namely Si-O-Zn (Shaba et al., 2023). This phenomenon may be linked to the formation of interfacial Si-O-Zn bonds that alter local atomic coordination and inhibit ZnO lattice development. The electron affinity of the Si ion, which has a positive value (+134.068 J mol⁻¹), is higher than that of the Zn²⁺ ion (-58 J mol⁻¹). As a result, Zn²⁺ tend to interact more with O²⁻ (+140.976 J mol⁻¹) rather than with the Si ion. From an electronic perspective, the relative electron affinities of and Zn^{2+} influence their bonding preferences and interaction with lattice oxygen, indirectly impacting crystallite evolution and defect formation (Sreenath et al., 2020). This interplay between attractive and repulsive forces enhances the diffusivity of O2 and Zn ions, thereby promoting the electron movement within the molecules and leading to smaller crystal sizes as the SiO₂ increases (Sreenath et al., 2020)(Qomariyah et al., 2020). Consequently, the nanocomposite exhibits not only finer crystallite domains but also improved surface defect

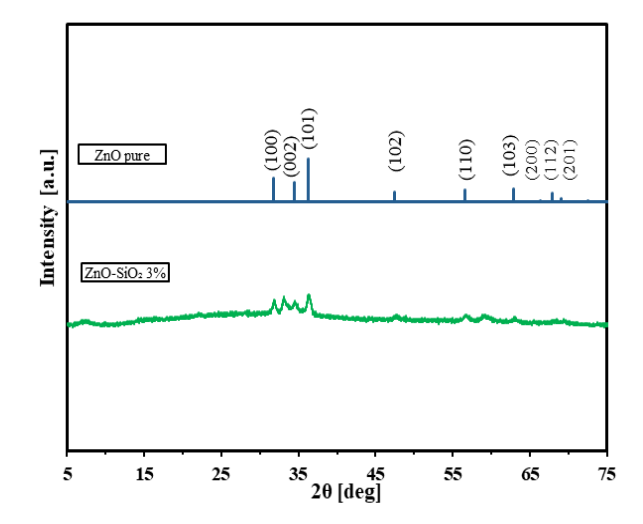


Fig 3. XRD result of pure ZnO and nanocomposite prepared at 45 Minutes Sonication Time

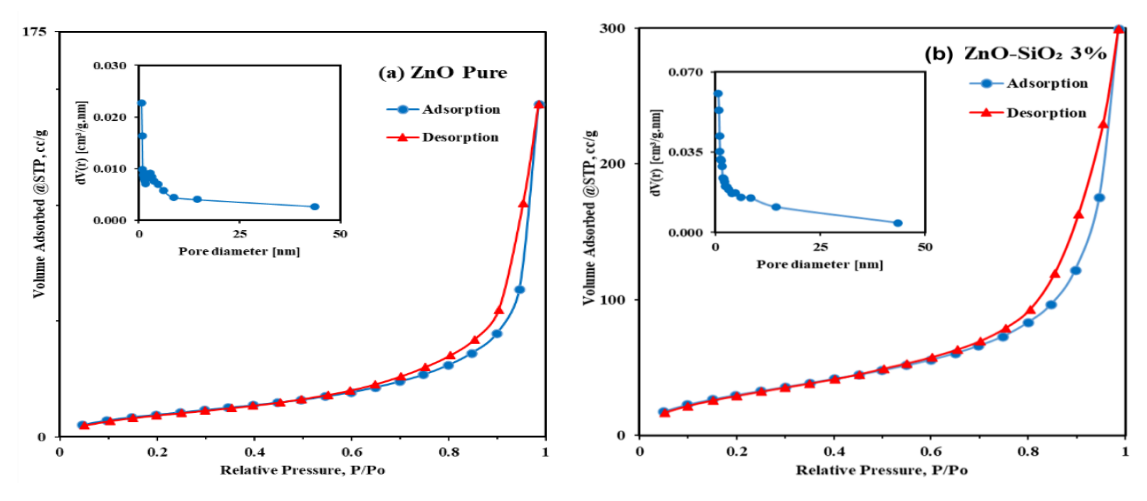


Fig 4. Adsorption-Desorption Isotherm Graph at 45 Minutes Sonication with SiO₂ Concentration (a) 0%, (b) 3%

Table 1BET Test Results of ZnO pure and nanocompoiste prepared at 45 Minutes Ultrasonication

Sample	S _{BET} (m ² /g)	Pore Volume (cm³/g)	Particle Diameter (nm)	Pore Diameter (nm)
ZnO Pure	3891	0.23	35.04	14.40
ZnO-SiO ₂ 3%	117.64	0.46	11.59	7.89

distribution—features that are beneficial for charge separation in photocatalysis.

The crystal size affects the surface area of the nanocomposite (Zhang et al., 2023) and BET (Brunauer-Emmett-Teller) testing has been conducted to estimate the properties, (including specific surface area, pore volume, and pore diameter) of the ZnO-SiO₂ nanocomposite. Smaller crystallites generally exhibit higher specific surface areas due to their larger surface-to-volume ratio, a factor directly linked to increased catalytic activity and adsorption capacity (Zhang et al., 2023). This test is important in material characterization because a high surface area correlates with catalytic activity and good adsorption properties, which are highly desirable in various industrial and technological applications. The results of the nitrogen adsorption-desorption BET test are shown in Fig. 4 and Table 1.

3.4. Surface Area and Porosity Analysis (BET): Isotherm Behaviour, Hysteresis Classification, Ultrasonication Influence, and Data Interpretation

In Figure 4, the nitrogen adsorption-desorption isotherm profiles and pore diameter distribution for the ZnO pure and ZnO-SiO $_2$ nanocomposite. Each sample is classified as having mesopore diameters (<50 nm). The pore size refers to the width of the pore, measured as the distance between two opposing walls. Accurate pore size measurements depend on the well-defined geometric shape of the pores. In this study, all samples showed pore diameters within the mesoporous range (2–50 nm), which is favourable for the diffusion and retention of dye molecules during photocatalytic degradation. Porosity is the ratio of the volume of pores and cavities to the total volume of the solid material and is closely linked to its adsorption properties.

Based on the IUPAC adsorption isotherm classification the adsorption-desorption isotherm graph shows type IV which

indicates that the pore diameter of the material is mesoporous. While particles with microporous pore diameters are indicated by type I; non-porous or macro-porous in types II , III , and VI; and meso-porous in types IV and V (Alothman, 2012). Type IV isotherms are also indicative of capillary condensation in mesopores and typically exhibit hysteresis loops, further confirming the pore structure of the synthesized nanocomposite.

IUPAC classifies hysteresis into several types (H1, H2, H3, H4), each reflecting different pore characteristics. Type H1 is typically associated with porous materials that have regular cylindrical pore channels or nearly uniform spherical aggregates. Type H2 refers to materials that are often irregular with uncertain pore sizes and shapes, indicating the presence of constrictions. Type H3 has slit-shaped pores and does not show an adsorption boundary at high P/Po, often found in non-rigid particle aggregates resembling plates. Meanwhile, H4-type hysteresis is commonly linked to narrow slit-shaped pores. Each sample tested exhibited a trend in the graph resembling type H3. Materials causing H3 hysteresis have long slit-shaped pores. The presence of H3 hysteresis loops suggests that the ZnO-SiO₂ nanocomposites likely form aggregated plate-like particles or layered pore structures that restrict desorption at high relative pressures.

Hysteresis in the BET isothermal test refers to the difference between the adsorption and desorption curves when measuring the quantity of gas absorbed by porous materials at various partial pressures at a constant temperature. Hysteresis curves appear when the path followed during adsorption differs from the path followed during desorption. This means that at the same partial pressure, the amount of gas adsorbed is not equal to the amount of gas desorbed. This form of hysteresis is often observed in materials with larger and more complex pores, such as mesopores and macropores, where capillary condensation occurs. In mesopores, gas can condense in the pores at lower pressures during desorption compared to

adsorption. (Alothman, 2012). The $\rm ZnO\textsc{-}SiO_2$ 3% sample has the smallest particle diameter, resulting a large surface area. This increased surface area enhances the availability of reactive sites for photocatalytic interactions, a desirable feature in dye degradation and environmental remediation. The increased surface area following the creation of the nanocomposite suggests that the synthesis of the $\rm ZnO\textsc{-}SiO_2$ nanocomposite indicates that its formation introduces additional active sites, leading to the inference that the sol-gel method supports the development of a well-structured and widely dispersed ZnO lattice within the $\rm SiO_2$ matrix (Shaba *et al.*, 2023).

The sonication process plays a role in the dispersion and homogenization of particles, which affects the final surface area of the nanocomposite. The dispersed silica with increased ultrasonication time reduces the agglomeration of ZnO, thereby increasing the surface area of the nanoparticles. Consistent with the role of ultrasonic treatment in enhancing porosity, the vibration and cavitation effects generated during sonication significantly promote surface enlargement and pore development, primarily by increasing the mesopore volume and micropore surface area. Thus, optimizing ultrasonic parameters is crucial to maximizing active site availability and ensuring a well-developed porous network in nanocomposite materials (Qomariyah *et al.*, 2020).

3.5. Morphological Characterization (SEM): Microstructure, SiO_2 Stabilization, Ultrasonic Dispersion, and Correlation with FTIR-XRD Analyses

The SEM image in Fig. 5 illustrates the morphology of the $\rm ZnO\textsc{-}SiO_2$ nanocomposite created through ultrasonication. The image reveals a porous and irregular network structure, typical of the aggregated $\rm ZnO$ and $\rm SiO_2$ particles. The SEM analysis verifies the presence of both $\rm SiO_2$ and $\rm ZnO$, demonstrated by the heterogeneous surface featuring various granular characteristics and layered structures. The particles appear interconnected in a loose network, suggesting that ultrasonication effectively disrupted hard agglomerates, allowing $\rm SiO_2$ to form a scaffold-like structure embedding $\rm ZnO$.

The porous nature of the observed morphology can be attributed to the formation of SiO_2 surrounding ZnO nanoparticles, leading to a networked composite structure. This morphology is advantageous for photocatalytic applications, as it provides a higher surface area that enhances light absorption and photocatalytic activity. The visible thin sheet-like and granular structures are indicative of the coexistence of silica and

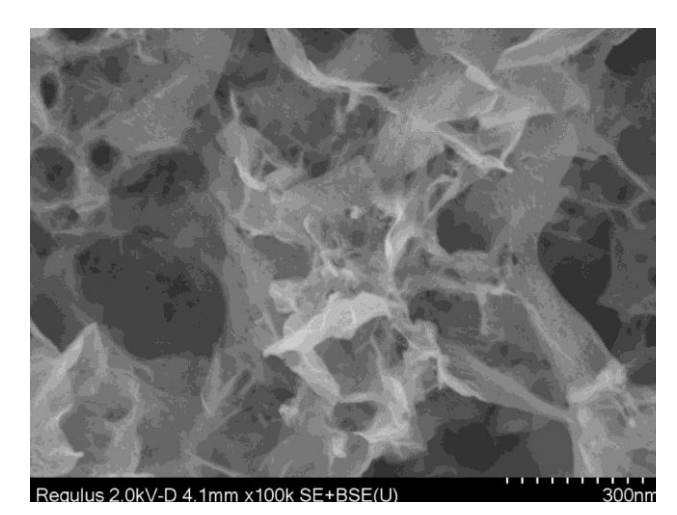


Fig 5. SEM image of ZnO-SiO₂

zinc oxide phases, supporting the effective incorporation of SiO₂ into the ZnO matrix (Kusdianto *et al.*, 2020).

These sheet-like features are likely formed by aggregated silica, while ZnO appears as smaller granules distributed along their surface. This supports the hypothesis that SiO₂ acts as a stabilizing matrix that prevents ZnO particle growth and (Raha & Ahmaruzzaman, 2022). coalescence morphological observation aligns well with XRD and also FTIR analysis, which confirmed the successful formation of the ZnO-SiO₂ nanocomposite. XRD revealed diffraction peaks associated with both ZnO and SiO2, while FTIR spectra showed characteristic bands confirming chemical bonding and the successful integration of ZnO with SiO2. These combined findings suggest that the structural assembly of the nanocomposite is consistent across molecular (FTIR), crystal (XRD), and morphological (SEM) levels, indicating reliable synthesis quality. The SEM micrograph thus complements these analyses, validating the structural formation and distribution of the composite materials. The ultrasonication process appears to contribute effectively to dispersing ZnO within the SiO₂ matrix, preventing severe agglomeration and leading to a more homogeneous distribution of the composite materials, as reflected in the morphological features. This process generates localized cavitation, which promotes shear forces and turbulence in the solution—factors that facilitate uniform dispersion of ZnO and reduce secondary particle growth. This uniform dispersion is critical for optimizing photocatalytic performance by ensuring consistent exposure to light and reactants. These results collectively demonstrate the effectiveness of the synthesis method in achieving a wellintegrated ZnO-SiO₂ nanocomposite suitable for photocatalytic applications (Fatimah et al., 2021). Ultimately, the well-defined porous morphology and particle distribution observed under SEM reinforce the suitability of ultrasonically synthesized ZnO-SiO₂ for use in dye degradation and environmental remediation technologies.

3.6. Photocatalytic Performance of $ZnO\text{-}SiO_2$ Nanocomposites in the Methylene Blue degradation.

The application of $\rm ZnO\textsc{-}SiO_2$ Nanocomposite as a photocatalyst material has been tested directly under sunlight. The preparation of a standard curve of MB using a concentration of 0-10 ppm at 663 nm wavelength was carried

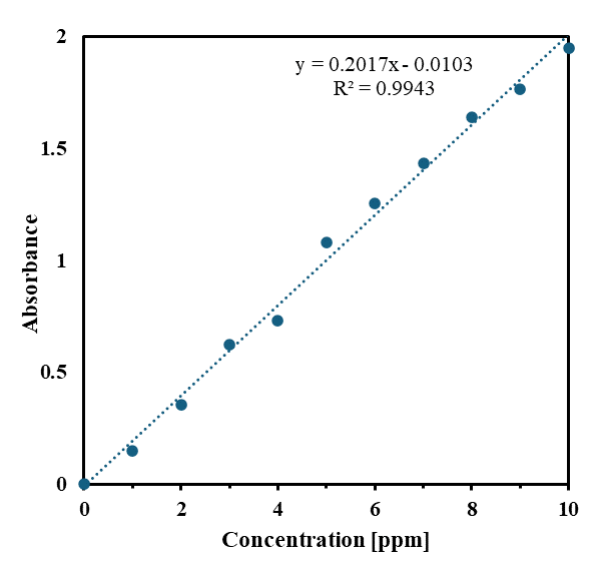


Fig 6. Standard Curve of Methylene Blue

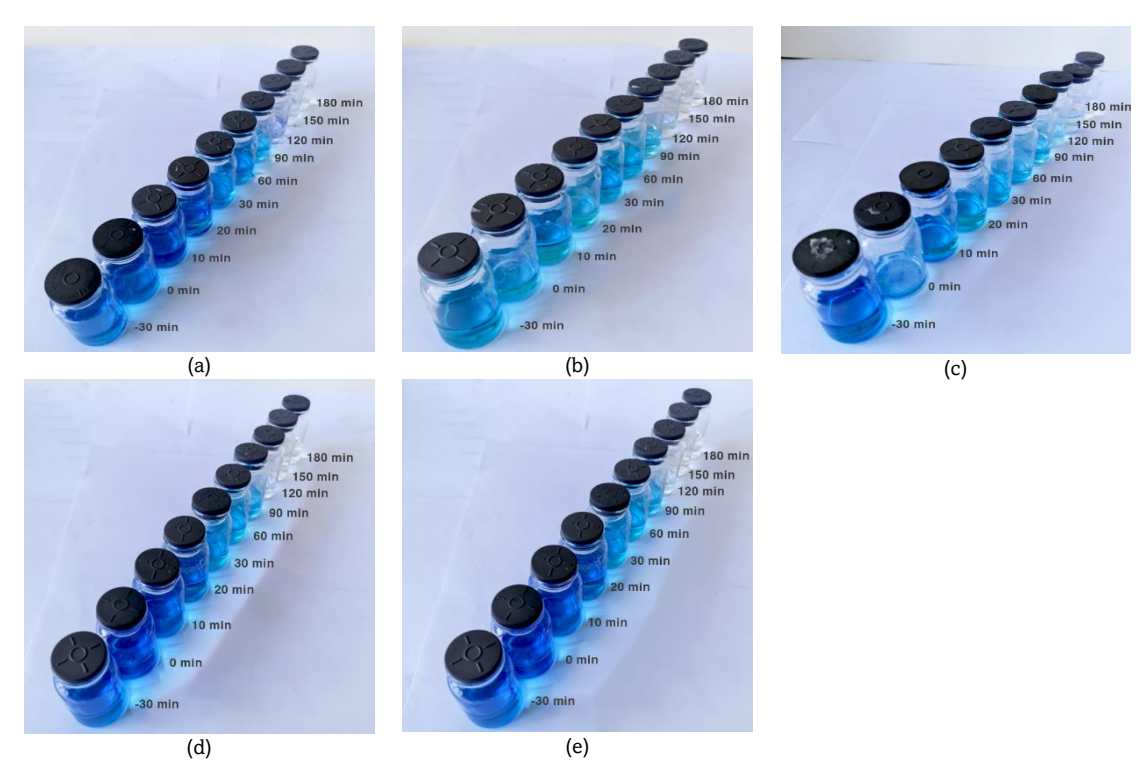


Fig 7. Methylene blue degradation using ZnO-SiO₂ prepared at various ultrasonication time (a) 0 minutes, (b) 10 minutes, (c) 20 minutes, (d) 30 minutes, and (e) 45 minutes.

out before the photocatalytic test of $ZnO\text{-}SiO_2$ Nanocomposite. The results of the standard curve are shown in Figure 6 . The results of the standard solution preparation obtained are in accordance with Lambert-Beer's law, which indicates that the absorbance value is directly correlated with the solution concentration. From the preparation of standard solutions with concentrations of 0-10 ppm, the equation obtained is y=0.2017x-0.0103, where the value of y represents absorbance and the value of x is the concentration of MB. The concentration of the photocatalytic results will be obtained by substituting the absorbance value of the photocatalytic results into y, allowing the value of x or the concentration of methylene blue to be determined. The correlation coefficient (R²) for this equation is 0.9943, indicating a high degree of linearity between absorbance and concentration.

The methylene blue degradation test using the $\rm ZnO\textsc{-}SiO_2$ nanocomposite was conducted with the aid of sunlight with a light intensity of 110,000-120,000 lux. The photocatalytic testing was performed in the dark for 30 minutes to determine the degradation capability without light, followed by exposure to sunlight until the methylene blue was degraded. The methylene blue degradation process using the $\rm ZnO\textsc{-}SiO_2$ nanocomposite with variations in ultrasonication time can be observed through changes in the intensity of the MB color in the photocatalytic results, as shown in Fig. 7.

Photocatalytic samples were taken at 0, 10, 20, 30, 60, 90, 120, 150, and 180 minutes. At 0 minute, the sample was taken immediately after the 30-minute dark condition, followed by photocatalysis using sunlight for the specified time intervals. Visually, the sample with a composition of 3% SiO₂ was capable of degrading methylene blue. UV-Vis absorbance analysis confirmed that the ZnO–SiO₂ nanocomposite (3 wt% SiO₂, 45 minutes ultrasonication) achieved 95% degradation efficiency of methylene blue under sunlight after 120 minutes. This high

degradation rate indicates effective charge separation and active surface exposure, supported by the nanostructure morphology and reduced agglomeration. During this time, the sample with a composition of 3% SiO₂ and an ultrasonication time of 45 minutes showed a lower color intensity. The fading of color intensity reflects the breakdown of chromophoric groups within the methylene blue structure, demonstrating successful photocatalytic degradation by the nanocomposite. This performance is consistent with previous studies showing that SiO₂-modified ZnO enhances pollutant degradation due to increased surface hydroxylation and reduced electron–hole recombination (Dedova *et al.*, 2020). Moreover, sunlight-driven catalysis using ZnO-based composites has been increasingly favored as a green alternative for wastewater treatment (Chalatsi-diamanti *et al.*, 2025; Dehghani *et al.*, 2022).

The absorbance graph above shows that as the absorbance value increases, the concentration of MB also increases. From Fig. 8, it is evident that at all ultrasonication time variables, the color of methylene blue can be degraded within 180 minutes. The results indicate that the MB degradation rate at a concentration of 10 ppm increases as the concentration of the solution decreases. Supplementary examination involved computing the rate constant (k) of the photocatalyst. The kinetics of methylene blue degradation at varying ultrasonication times are illustrated in Fig. 9.

The degradation kinetics were calculated using the Langmuir-Hinshelwood model. Figure 9 illustrates the results showing fluctuating k values as the ultrasonication time varies. The nanocomposite with a $\rm SiO_2$ content of 3% and an ultrasonication time of 0 minutes recorded the peak (k) value of 0.0255 min⁻¹. The photocatalytic activity of $\rm ZnO\textsc{-}SiO_2$ nanocomposites was evaluated by the MB degradation under sunlight, achieving the best performance of 97% under 45 minutes of ultrasonication. To provide a clearer overview of this

trend, Table 2 presents the degradation rates of methylene blue for the nanocomposites with 3% ${\rm SiO_2}$ under different

ultrasonication durations

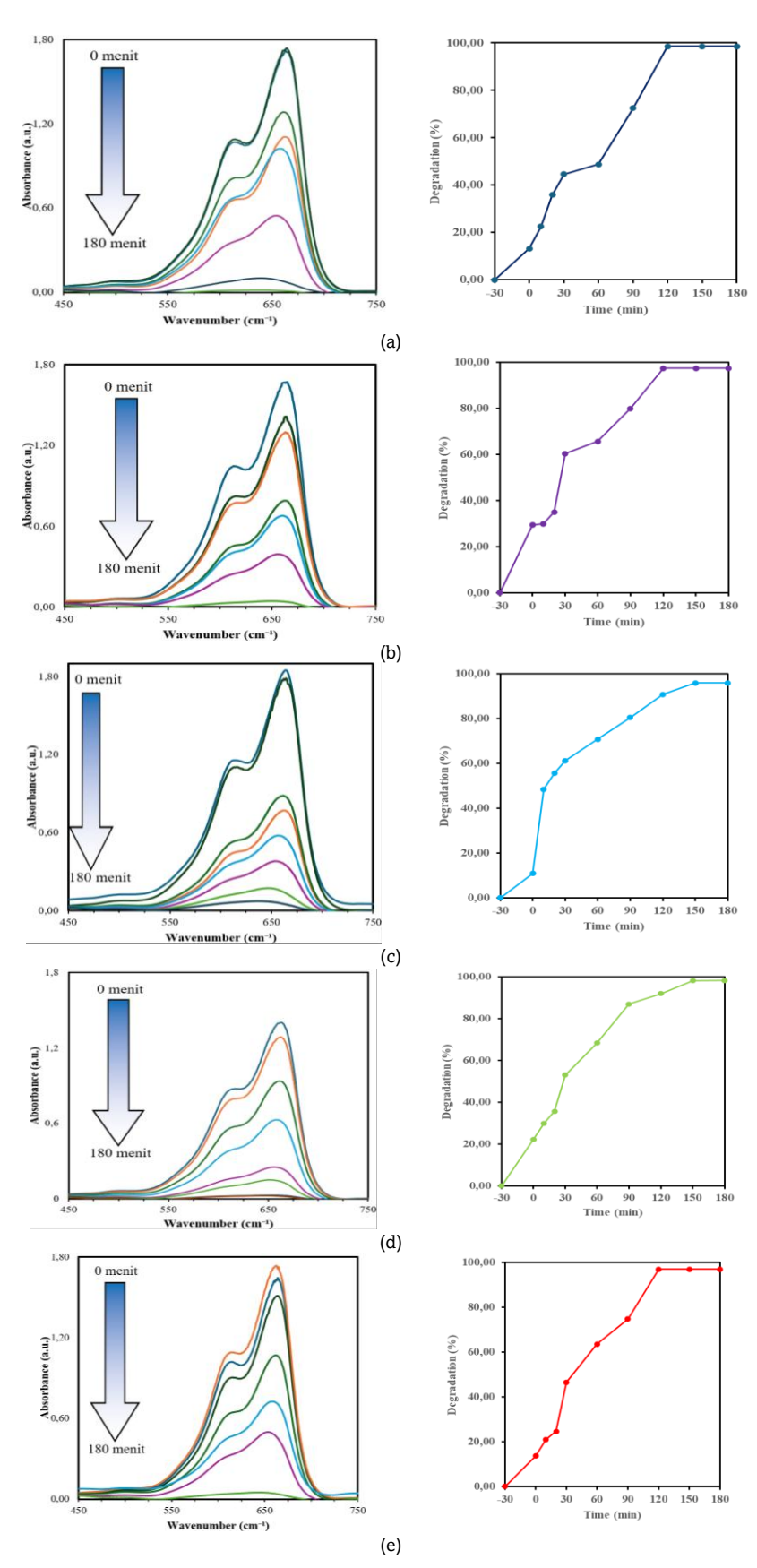


Fig 8 Absorbance spectra of the ZnO-SiO₂ prepared under various ultrasonication time (a) 0, (b) 10, (c) 20, (d) 30, and (e) 45 minutes

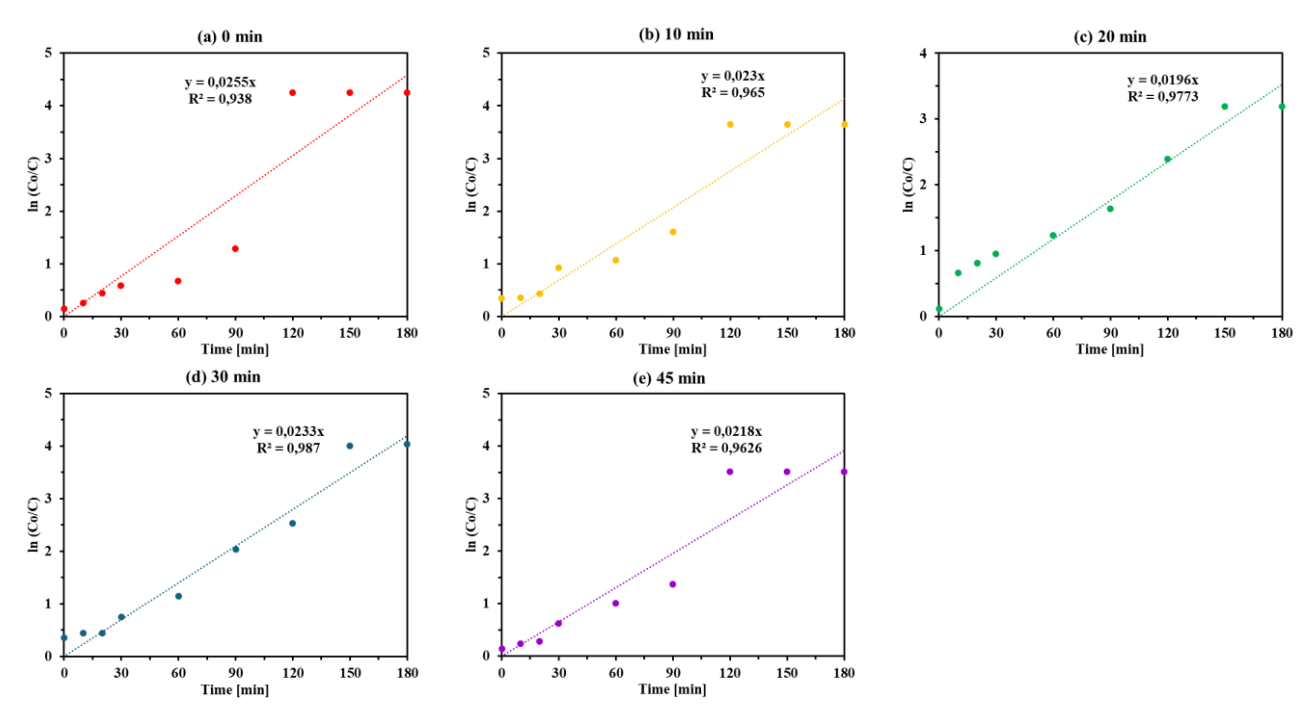


Fig 9 $ln(C_0/C_t)$ as a function of MB Degradation using $ZnO-SiO_2$ under various ultrasonication time (a) 0, (b), 10, (c) 20, (d) 30, and (e) 45 minutes

Table 2Degradation Rate of Methylene Blue at 3% SiO. Concentration Variation of Ultrasonication Time

0 98.58 0.0255 10 97.40 0.0230 20 95.90 0.0196 30 98.23 0.0233	Ultrasonication Time (min)	Max Degradation (%)	Degradation rate constant (min ⁻¹)	
10 97.40 0.0230 20 95.90 0.0196	0			
20 95.90 0.0196	10			
50 90.25 0.0255				
45 97.02 0.0218				

4. Conclusion

This study successfully optimized the ultrasonication time in the production of $\rm ZnO\textsc{-}SiO_2$ nanocomposites, demonstrating its significant impact on the characteristics and photocatalytic performance of the material. The synthesis process utilizing the sol-gel method for silica preparation, and followed with the incorporation of $\rm ZnO$, effectively mitigated issues of particle agglomeration and allowed for the control of particle size at the nanoscale. Through various ultrasonication durations, it was determined that an optimal ultrasonication time of 45 minutes resulted in the highest quality $\rm ZnO\textsc{-}SiO_2$ nanoparticles, as evidenced by FTIR, XRD, and SEM analyses.

The characterization results indicated the successful formation of $\rm ZnO\textsc{-}SiO_2$ nanoparticles with a large surface area of 117.64 m²/g, moderate pore volume, and small pore diameter, which are crucial for enhancing photocatalytic performance. The photocatalytic degradation tests, specifically the degradation of methylene blue under sunlight, showed remarkable efficiency, achieving a degradation rate of 97% with the optimized ultrasonication time.

These results emphasize the effectiveness of the ultrasonication technique in producing highly efficient photocatalysts for potential industrial applications. The enhanced photocatalytic activity of the ZnO-SiO₂ nanocomposite presents promising opportunities for the development of advanced materials aimed at environmental remediation and other applications requiring effective

photocatalysts. Future studies could concentrate on optimizing the synthesis process and investigating further potential applications of ZnO-SiO_2 nanocomposites in various fields.

Acknowledgments

This work is financially supported in part by a grant from Directorate of Research and Public Service, Institut Teknologi Sepuluh Nopember (L.Q) under contract number 1252/PKS/ITS/2024.

References

Ali, A. M., Harraz, F. A., Ismail, A. A., Al-Sayari, S. A., Algarni, H., & Al-Sehemi, A. G. (2016). Synthesis of amorphous ZnO-SiO2 nanocomposite with enhanced chemical sensing properties. *Thin Solid Films*, 605, 277–282. https://doi.org/10.1016/j.tsf.2015.11.044

Alothman, Z. A. (2012). A review: Fundamental aspects of silicate mesoporous materials. *Materials*, 5(12), 2874–2902. https://doi.org/10.3390/ma5122874

Asadi, A., Pourfattah, F., Miklós Szilágyi, I., Afrand, M., Żyła, G., Seon Ahn, H., Wongwises, S., Minh Nguyen, H., Arabkoohsar, A., & Mahian, O. (2019). Effect of sonication characteristics on stability, thermophysical properties, and heat transfer of nanofluids: A comprehensive review. *Ultrasonics Sonochemistry*, 58, 104701.

https://doi.org/10.1016/J.ULTSONCH.2019.104701

Bindu, P., & Thomas, S. (2014). Estimation of lattice strain in ZnO

- nanoparticles: X-ray peak profile analysis. *Journal of Theoretical and Applied Physics*, 8(4), 123–134. https://doi.org/10.1007/s40094-014-0141-9
- Chalatsi-diamanti, P., Isari, E. A., Grilla, E., & Kokkinos, P. (2025).

 Recent prospects , challenges and advancements of photocatalysis as a wastewater treatment method. *Water Emerg. Contam.*Nanoplastics, 4(12). https://doi.org/10.20517/wecn.2025.03
- Chen, X., Wu, Z., Liu, D., & Gao, Z. (2017). Preparation of ZnO Photocatalyst for the Efficient and Rapid Photocatalytic Degradation of Azo Dyes. *Nanoscale Research Letters*, *12*(1). https://doi.org/10.1186/S11671-017-1904-4
- Chen, Y., Ding, H., & Sun, S. (2017). Preparation and characterization of ZnO nanoparticles supported on amorphous SiO2. Nanomaterials, 7(8). https://doi.org/10.3390/nano7080217
- Dedova, T., Acik, I. O., Chen, Z., Katerski, A., Balmassov, K., Gromyko, I., Nagyné-Kovács, T., Szilágyi, I. M., & Krunks, M. (2020). Enhanced photocatalytic activity of ZnO nanorods by surface treatment with HAuCl4: Synergic effects through an electron scavenging, plasmon resonance and surface hydroxylation. *Materials Chemistry and Physics*, 245, 2–11. https://doi.org/10.1016/j.matchemphys.2020.122767
- Dehghani, M., Naseri, M., Nadeem, H., Banaszak Holl, M. M., & Batchelor, W. (2022). Sunlight-driven photocatalytic per- and polyfluoroalkyl substances degradation over zinc oxide/cellulose nanofiber catalyst using a continuous flow reactor. *Journal of Environmental Chemical Engineering*, 10(6), 108686. https://doi.org/10.1016/j.jece.2022.108686
- El Golli, A., Contreras, S., & Dridi, C. (2023). Bio-synthesized ZnO nanoparticles and sunlight-driven photocatalysis for environmentally-friendly and sustainable route of synthetic petroleum refinery wastewater treatment. *Scientific Reports*, *13*(1), 1–14. https://doi.org/10.1038/s41598-023-47554-2
- Elbanna, O., Zhang, P., Fujitsuka, M., & Majima, T. (2016). Facile preparation of nitrogen and fluorine codoped TiO2 mesocrystal with visible light photocatalytic activity. *Applied Catalysis B: Environmental,* 192, 80–87. https://doi.org/10.1016/j.apcatb.2016.03.053
- Faizah, N., & Qomariyah, L. (2024). A Review on Recent Progress in Material Design Using Spray Drying Technology —An Experimental and Theoretical Study—. Earozoru Kenkyu, 39(4), 249–262. https://doi.org/10.11203/jar.39.249
- Faizah, N., Widiyastuti, W., Setyawan, H., & Nurtono, T. (2024). Extraction of antioxidant and antibacterial agents from avocado (Persea americana) seed using Pulsed Electric Field method. *Industrial Crops and Products*, 222(P3), 119803. https://doi.org/10.1016/j.indcrop.2024.119803
- Fatimah, I., Fadillah, G., Sahroni, I., Kamari, A., Sagadevan, S., & Doong, R. A. (2021). Nanoflower-like composites of ZnO/SiO2 synthesized using bamboo leaves ash as reusable photocatalyst. *Arabian Journal of Chemistry*, 14(3), 102973. https://doi.org/10.1016/j.arabjc.2020.102973
- Holder, C. F., & Schaak, R. E. (2019). Tutorial on Powder X-ray Diffraction for Characterizing Nanoscale Materials. *ACS Nano*, 13(7), 7359–7365. https://doi.org/10.1021/acsnano.9b05157
- Jin, J., Ma, H., Wang, K., Yagoub, A. E. G. A., Owusu, J., Qu, W., He, R., Zhou, C., & Ye, X. (2015). Effects of multi-frequency power ultrasound on the enzymolysis and structural characteristics of corn gluten meal. *Ultrasonics Sonochemistry*, 24, 55–64. https://doi.org/10.1016/j.ultsonch.2014.12.013
- Joshaghani, M., Yazdani, D., & Zinatizadeh, A. A. (2017). Statistical modeling of p-nitrophenol degradation using a response surface methodology (RSM) over nano zero-valent iron-modified Degussa P25-TiO2/ZnO photocatalyst with persulfate. *Journal of the Iranian Chemical Society*, 14(11), 2449–2456. https://doi.org/10.1007/s13738-017-1179-9
- Kadir, A., Qomariyah, L., Ogi, T., Atmajaya, H., Putra, N. R., Sunarno, S. D. A. M., Tejamaya, M., & Zuchrillah, D. R. (2023). Cost-effective and rapid synthesis of ZnO photocatalyst with the high performance of dye photodegradation as application in minimizing chemical risks used in industry. *Journal of Sol-Gel Science and Technology*, 107(3), 711–724. https://doi.org/10.1007/s10971-023-06147-1
- Kurnaz Yetim, N., Kurşun Baysak, F., Koç, M. M., & Nartop, D. (2020).

- Characterization of magnetic Fe3O4@SiO2 nanoparticles with fluorescent properties for potential multipurpose imaging and theranostic applications. *Journal of Materials Science: Materials in Electronics*, 31(20), 18278–18288. https://doi.org/10.1007/s10854-020-04375-7
- Kusdianto, K., Widiyastuti, W., Shimada, M., Qomariyah, L., & Winardi, S. (2020). Fabrication of ZnO-SiO2 Nanocomposite Materials Prepared by a Spray Pyrolysis for the Photocatalytic Activity under UV and Sunlight Irradiations. IOP Conference Series: Materials Science and Engineering, 778(1). https://doi.org/10.1088/1757-899X/778/1/012105
- Lee, K. M., & Abd Hamid, S. B. (2015). Simple response surface methodology: Investigation on advance photocatalytic oxidation of 4-chlorophenoxyacetic acid using UV-active ZnO photocatalyst. *Materials*, 8(1), 339–354. https://doi.org/10.3390/ma8010339
- Mahdavi, R., & Ashraf Talesh, S. S. (2017). The effect of ultrasonic irradiation on the structure, morphology and photocatalytic performance of ZnO nanoparticles by sol-gel method. *Ultrasonics Sonochemistry*, 39(February), 504–510. https://doi.org/10.1016/j.ultsonch.2017.05.012
- Mourya, A. K., Singh, R. P., Kumar, T., Talmale, A. S., Gaikwad, G. S., & Wankhade, A. V. (2023). Tuning the morphologies of ZnO for enhanced photocatalytic activity. *Inorganic Chemistry Communications*, 154(May), 110850. https://doi.org/10.1016/j.inoche.2023.110850
- Ortiz-Quiñonez, J. L., & Pal, U. (2024). Interface engineered metal oxide heterojunction nanostructures in photocatalytic CO2 reduction: Progress and prospects. *Coordination Chemistry Reviews*, 516(January). https://doi.org/10.1016/j.ccr.2024.215967
- Qomariyah, L., Widiyastuti, W., Kusdianto, K., Nurtono, T., Anggoro, D., & Winardi, S. (2020). Rapid electrospray synthesis and photocatalytic activities inhibition by ZnO-SiO 2 composite particles. *Chemical Papers*, 74, 4115–4123.
- Qu, W., Ma, H., Jia, J., He, R., Luo, L., & Pan, Z. (2012). Enzymolysis kinetics and activities of ACE inhibitory peptides from wheat germ protein prepared with SFP ultrasound-assisted processing. *Ultrasonics Sonochemistry*, 19(5), 1021–1026. https://doi.org/10.1016/j.ultsonch.2012.02.006
- Raha, S., & Ahmaruzzaman, M. (2022). ZnO nanostructured materials and their potential applications: progress, challenges and perspectives. *Nanoscale Advances*, 4(8), 1868–1925. https://doi.org/10.1039/d1na00880c
- Ren, X., Ma, H., Mao, S., & Zhou, H. (2014). Effects of sweeping frequency ultrasound treatment on enzymatic preparations of ACE-inhibitory peptides from zein. European Food Research and Technology, 238(3), 435–442. https://doi.org/10.1007/s00217-013-2118-3
- Rohilla, S., Gupta, A., Kumar, V., Kumari, S., Petru, M., Amor, N., Noman, M. T., & Dalal, J. (2021). Excellent UV-Light Triggered Photocatalytic Performance of ZnO.SiO2 Nanocomposite for Water Pollutant Compound Methyl Orange Dye. *Nanomaterials*, 11(10), 2548. https://doi.org/10.3390/nano11102548
- Selvinsimpson, S., Gnanamozhi, P., Pandiyan, V., Govindasamy, M., Habila, M. A., AlMasoud, N., & Chen, Y. (2021). Synergetic effect of Sn doped ZnO nanoparticles synthesized via ultrasonication technique and its photocatalytic and antibacterial activity.

 Environmental Research, 197, 111115. https://doi.org/10.1016/j.envres.2021.111115
- Shaba, E. Y., Tijani, J. O., Jacob, J. O., & Suleiman, M. A. T. (2023). Effect of mixing ratios of SiO2 nanoparticles synthesized from metakaolin on the physicochemical properties of ZnO/SiO2 nanocomposites. *Nano-Structures and Nano-Objects*, 35, 101003. https://doi.org/10.1016/j.nanoso.2023.101003
- Sreenath, P. R., Mandal, S., Panigrahi, H., Das, P., & Dinesh Kumar, K. (2020). Carbon dots: Fluorescence active, covalently conjugated and strong reinforcing nanofiller for polymer latex. Nano-Structures and Nano-Objects, 23, 100477. https://doi.org/10.1016/j.nanoso.2020.100477
- Stanley, R., J, A. J., & S, M. V. (2019). Enhanced sunlight photocatalytic degradation of methylene blue by rod-like ZnO-SiO2 nanocomposite. *Optik*, *180*(November 2018), 134–143. https://doi.org/10.1016/j.ijleo.2018.11.084
- Wang, D., Yan, L., Ma, X., Wang, W., Zou, M., Zhong, J., Ding, T., Ye,

- X., & Liu, D. (2018). Ultrasound promotes enzymatic reactions by acting on different targets: Enzymes, substrates and enzymatic reaction systems. *International Journal of Biological Macromolecules*, 119, 453–461. https://doi.org/10.1016/j.ijbiomac.2018.07.133
- Wang, J., Shah, Z. H., Zhang, S., & Lu, R. (2014). Silica-based nanocomposites via reverse microemulsions: Classifications, preparations, and applications. *Nanoscale*, 6(9), 4418–4437. https://doi.org/10.1039/c3nr06025j
- Wang, M., Zhang, M., Pang, L., Yang, C., Zhang, Y., Hu, J., & Wu, G. (2019). Fabrication of highly durable polysiloxane-zinc oxide (ZnO) coated polyethylene terephthalate (PET) fabric with improved ultraviolet resistance, hydrophobicity, and thermal resistance. *Journal of Colloid and Interface Science*, 537, 91–100. https://doi.org/10.1016/j.jcis.2018.10.105
- Wang, N., Yang, Y., & Yang, G. (2011). Great blue-shift of luminescence of ZnO nanoparticle array constructed from ZnO quantum dots.

 Nanoscale Research Letters, 6(1), 2–7. https://doi.org/10.1186/1556-276X-6-338
- Wang, X., Zhou, S., & Wu, L. (2013). Facile encapsulation of SiO2 on

- ZnO quantum dots and its application in waterborne UV-shielding polymer coatings. *Journal of Materials Chemistry C*, *1*(45), 7547–7553. https://doi.org/10.1039/c3tc31479k
- Winardi, S., Qomariyah, L., Widiyastuti, W., Kusdianto, K., Nurtono, T., & Madhania, S. (2020). The role of electro-sprayed silica-coated zinc oxide nanoparticles to hollow silica nanoparticles for optical devices material and their characterization. *Colloids and Surfaces A: Physicochemical and Engineering Aspects*, 604(February), 125327. https://doi.org/10.1016/j.colsurfa.2020.125327
- Xu, B., Azam, S. M. R., Feng, M., Wu, B., Yan, W., Zhou, C., & Ma, H. (2021). Application of multi-frequency power ultrasound in selected food processing using large-scale reactors: A review. *Ultrasonics Sonochemistry*, 81, 105855. https://doi.org/10.1016/j.ultsonch.2021.105855
- Zhang, K., Wang, J., Ninakanti, R., & Verbruggen, S. W. (2023).

 Solvothermal synthesis of mesoporous TiO2 with tunable surface area, crystal size and surface hydroxylation for efficient photocatalytic acetaldehyde degradation. *Chemical Engineering Journal*, 474(May), 145188. https://doi.org/10.1016/j.cej.2023.145188



© 2025. The Author(s). This article is an open access article distributed under the terms and conditions of the Creative Commons Attribution-ShareAlike 4.0 (CC BY-SA) International License (http://creativecommons.org/licenses/by-sa/4.0/)